Casein Phosphopeptide-Amorphous Calcium Phosphate Nanocomplexes: A Structural Model

Keith J. Cross, N. Laila Huq, Eric C. Reynolds*

Oral Health CRC, Melbourne Dental School, Bio21 Institute, The University of Melbourne, 720 Swanston Street, Melbourne, Victoria, 3010, Australia.

KEYWORDS. Biomineralisation; phosphoprotein; amorphous calcium phosphate; milk micelles

RUNNING TITLE: Characterisation of Casein Phosphopeptide-Amorphous Calcium Phosphate

*Corresponding author: Eric C. Reynolds. Email: e.reynolds@unimelb.edu.au

1

ABBREVIATIONS

ACP, amorphous calcium phosphate; CN, casein; CPP, casein phosphopeptides; DQF-COSY, double-quantum filtered correlation spectroscopy; NOESY, nuclear Overhauser effect spectroscopy; Ser(P) andPse, O-phosphoserine; TOCSY, total correlation spectroscopy; Tris, tris(hydroxymethylaminomethane).

1
2
3
4
5
6
7
8
9
10
11
12
13
14
15
16
17
18
19
20
21
22
23
24
25
26
27
28
29
30
31
32
33
34
35
36
37
38
39
40
41
42
43
44
45
46
47
48
49
50
51
52
53
54
55
56
57
58
59
60

ABSTRACT

Tryptic digestion of the calcium-sensitive caseins yields casein phosphopeptides (CPP) that contain clusters of phosphorylated seryl residues. The CPP stabilize calcium and phosphate ions through the formation of complexes. The calcium phosphate in these complexes is biologically available for intestinal absorption and remineralisation of subsurface lesions in tooth enamel. We have studied the structure of the complexes formed by the CPP with calcium phosphate using a variety of NMR techniques. Translational diffusion measurements indicated that the β-CN(1-25)–ACP nanocomplex has a hydrodynamic radius of 1.526 ± 0.044 nm at pH 6.0 increasing to 1.923 ± 0.082 nm at pH 9.0. ^{1}H NMR spectra were well resolved and $^{3}J_{H^{N}}$-$_{H^{\alpha}}$ measurements ranged from a low of 5.5 Hz to a high of 8.1 Hz. TOCSY and NOESY spectra were acquired and sequentially assigned. Experiments described in this paper have allowed the development of a structural model for the β-CN(1-25)-amorphous calcium phosphate nanocomplex.

3

Bovine milk contains approximately 30 mM calcium and 22 mM inorganic phosphate in solution with most of the calcium (68%) and phosphate (47%) associated with the proteins α_{S1}-, α_{S2}-, β- and κ-casein in casein micelles [1, 2]. The α_{S1}-, α_{S2}-, and β-caseins have a number of Ser(P) residues in specific phosphorylation-site motifs, such as [-(Ser(P)-)$_3$(Glu-)$_2$], that are essential for their interaction with calcium phosphate [3].

There have been many studies of the ultrastructure of casein micelles using a variety of techniques [4, 5] with more recent studies using small-angle X-ray scattering [6] and electron microscopy [7]. Although the structural details are still being elucidated, the casein micelles are believed to be roughly spherical particles with a radius of about 100 nm, dispersed in a continuous phase of water, salt, lactose and whey proteins [8]. The calcium phosphate isolated after exhaustive hydrazine deproteination of micelles has been reported to exhibit a fine and uniform granularity under the electron microscope with the particles consisting of small subunits of 2.5 nm diameter [9]. The calcium phosphate, present as nanometer-sized ion clusters, and caseins are not covalently bound, hence the casein micelle is known as an association colloid [10]. Nevertheless, the casein micelles are extremely stable and can withstand boiling, freeze-drying and the addition of salt and ethanol. It is believed that the amphipathic, glycosylated C-terminal end of κ-casein protrudes from the micelle surface forming a so-called 'hairy layer' that sterically stabilizes the complexes [11].

The casein micelles serve as a carrier of calcium phosphate providing the neonate with a bioavailable source of calcium and phosphate ions for bone and teeth formation [3]. The formation of stable casein - calcium phosphate complexes is thought to be part of a general mechanism for

4

regulating calcium flow in tissues and biological fluids containing high calcium ion concentrations[11].

The ability of casein micelles to maintain calcium and phosphate ions in a soluble and bioavailable state is retained by the tryptic multiphosphorylated peptides of the caseins known as the casein phosphopeptides (CPP) [12]. The major tryptic CPP are β-CN(1-25) [1] and α_{S1}-CN(59-79) [2] with smaller amounts of α_{S2}-CN(46-70) [3] and α_{S2}-CN(1-21) [4] [13, 14]. These peptides all contain the cluster sequence motif -(Ser(P)-)$_3$(Glu-)$_2$ with three contiguous phosphoserines. This peptide motif is thought to be critical for calcium and calcium phosphate binding by these peptides [12]. The sequences of the four major casein tryptic phosphopeptides are shown below with the motif underlined.

[1] Arg[1]-Glu-Leu-Glu-Glu-Leu-Asn-Val-Pro-Gly-Glu-Ile-Val-Glu-Ser(P)-Leu-(Ser(P)-)$_3$(Glu-)$_2$Ser-Ile-Thr-Arg[25]

   β-CN(1-25)

[2] Gln[59]-Met-Glu-Ala-Glu-Ser(P)-Ile-(Ser(P)-)$_3$(Glu-)$_2$Ile-Val-Pro-Asn-Ser(P)-Val-Glu-Gln-Lys[79]

   α_{S1}-CN(59-79)

[3] Asn[46]-Ala-Asn-Glu-Glu-Glu-Tyr-Ser-Ile-Gly-(Ser(P)-)$_3$(Glu-)$_2$Ser(P)-Ala-Glu-Val-Ala-Thr-Glu-Glu-Val-Lys[70]

   α_{S2}-CN(46-70)

[4]   Lys[1]-Asn-Thr-Met-Glu-His-Val-(Ser(*P*)-)$_3$(Glu-)$_2$Ser-Ile-Ile-Ser(*P*)-Gln-Glu-Thr-Tyr-Lys[21]

α_{S2}-CN(1-21)

The CPP stabilize calcium and phosphate ions forming metastable solutions that are supersaturated with respect to the solid calcium phosphate phases[15]. Under these conditions, the CPP bind their equivalent weight of calcium and phosphate[16]. The CPP are formed *in vivo* by normal digestion of casein and, as they are relatively resistant to further proteolytic degradation, accumulate in the distal portion of the small intestine[17-21]. It has been proposed that this accumulation together with the peptides' ability to form soluble complexes with calcium phosphate are responsible for the enhanced intestinal calcium absorption that has been observed even in vitamin D deficient animals consuming dietary CPP[17-21]. In addition, CPP increase the calcification of *in vitro* cultured embryonic rat bone and again the mechanism is suggested to be associated with the peptide's ability to form soluble complexes with calcium and phosphate ions[22]. Furthermore, CPP-calcium phosphate complexes have been shown to be anticariogenic and remineralise early stages of enamel caries in animal and human studies[12, 15, 23-25]. In summary, the ability to kinetically stabilize amorphous calcium phosphate against primary precipitation enhances mineral ion bioavailability[26] and confers upon the CPP the potential to be biological delivery vehicles for calcium and phosphate ions[27]. However, although various examples of CPP-calcium phosphate biological function have been documented, the supramolecular structure of these complexes has yet to be elucidated.

As part of our long-term investigation into the structure-function relationships of proteins involved in biomineralisation and calcium phosphate stabilization, we have studied the solution structures of tryptic phosphopeptides from milk caseins and their interaction with the amorphous

6

and crystalline phases of calcium phosphate[28-34]. In this paper, we report our ^{1}H NMR

spectroscopic investigations of the β-CN(1-25)–ACP nanocomplex. We present a detailed model

of the β-CN(1-25)–ACP nanocomplex consistent with the NMR spectroscopic information

presented in this paper and with results presented elsewhere[29, 30, 32-34].

EXPERIMENTAL PROCEDURES

Materials and Methods

Preparation of casein phosphopeptides. The casein phosphopeptides β-CN(1-25) and

α_{S1}-CN(59-79) were selectively precipitated from a tryptic digest of casein using calcium

chloride and ethanol and further purified by anion exchange FPLC and reversed phase HPLC[14].

The purity of the peptides was assessed by MALDI-TOF mass spectrometry, capillary

electrophoresis, amino acid composition and sequence analyses [13, 14]. Prior to sequence analysis,

the labile phosphoseryl residues were converted to *S*-ethyl cysteinyl residues by β-elimination[14].

Electrophoresis of cross-linked α_{S1}-CN(59-79). Three 50 μL samples of the peptide

α_{S1}-CN(59-79) in distilled water at a concentration of 10 g/L at pH 6.7 were preincubated for 1

hour at room temperature with (a) 0 mM CaCl$_2$, (b) 60 mM CaCl$_2$, or (c) 60 mM CaCl$_2$ and 60

mM K$_3$PO$_4$. After the addition of 2 μL of 0.5% v/v glutaraldehyde, the reaction mixtures were

incubated for a further 30 min prior to dilution with an equal volume of loading buffer containing

20% glycerol and 0.45 M EDTA. Native polyacrylamide gel electrophoresis was performed

7

using 1 mm thick 20% gels[35] with the Mini-PROTEAN II system (Bio-Rad), at 100 V for 5

hours, at 4 °C. Gels were then washed for 1 hour in 0.25% isopropanol to remove glycine, and

stained overnight with "Stains All" (Eastman-Kodak Co.)[36].

Preparation of CPP-calcium phosphate. CPP-ACP solutions were prepared as described

previously [37]

NMR Spectroscopy. All NMR spectra were acquired on a Varian [UNITY]Inova spectrometer

operating at a field strength of 599.741 MHz. Samples of β-CN(1-25) were prepared with

peptide concentrations ranging from 1.0 mM to 4.5 mM.

Translational diffusion coefficients were determined using the sLED technique [38] with CPP-

ACP samples dissolved in 99.96% D_2O solution. The diffusion coefficients were determined by

fitting the observed signal intensity, A, to the following expression

$$A(2t) = A(0)\exp\left[-\gamma^2 D\left(\Delta - \delta/3\right)\delta^2 G^2\right] \quad [1]$$

where γ is the gyromagnetic ratio for the proton and G is the applied gradient magnitude. The

magnetic field gradient duration, δ, was fixed at 5 ms, and the diffusion delay Δ was fixed at 50,

100 and 200 ms in successive experiments. The gradient amplitude, G, was varied from 0 to a

maximum of approximately 30 gauss cm^{-1}. The translational diffusion coefficients, D, are related

to effective hydrodynamic radii, a, by the Stokes-Einstein equation

$$D = \frac{kT}{6\pi a \eta} \quad [2]$$

8

where k is the Boltzmann constant, T is the absolute temperature, and η is the sample viscosity. In practice, these equations were combined and the sLED data were fitted to an equation of the form

$$A(2t) = A(0)\exp\left[-\alpha G^2 \big/ a\right] \qquad [3]$$

The parameter α contains the fundamental constants (γ, k), sample dependent constants (T, η), delays (δ, Δ), and a calibration term converting the applied spectrometer gradients (arbitrary units) to cgs units. The parameter α was determined using the HDO peak as an internal calibrant and assuming a hydrodynamic radius of 1.40 Å for the water molecule. Hydrodynamic radii of the CPP–ACP complexes were calculated using peak amplitude data from a number of resonances and also from peak integrals over selected portions of the NMR spectra.

Solvent exposure of protons in β-CN(1-25)–ACP was studied using the CLEANEX_PM pulse sequence [39]. The sample of β-CN(1-25)–ACP was prepared in 90% H_2O/ 10% D_2O. The only resonances expected to be observed in this experiment were from solvent exposed protons not participating in hydrogen-bonding networks.

Two-dimensional NMR Spectroscopy. Phase-sensitive DQF-COSY, TOCSY, and NOESY spectra were acquired using the States-Haberkorn method [40]. All spectra were acquired with spectral widths of 6000 Hz in F_2 and F_1. The DQF-COSY spectrum was acquired with 800-t_1 increments each of 2048 complex data points. The spectrum was zero-filled in t_2 and t_1 to yield a final data matrix of 4k by 2k real points on Fourier transformation. TOCSY and NOESY spectra were acquired with 80 to 140 t_1 increments each of 2048 complex data points. Spectra were zero-filled in t_2 and linear prediction used in t_1 to yield final data matrices of 2k by 2k real points on

9

Fourier transformation. Sine-bell window functions were used in both dimensions of the DQF-

COSY spectra, and sine-bell window functions shifted by $\pi/3$ were used in both dimensions for

TOCSY and NOESY spectra. The residues were assigned using the standard assignment protocol

[41] as modified by Chazin *et al.* [42].

Molecular modeling of β-CN(1-25)–ACP. For molecular modeling of the β-CN(1-25)–ACP

complex, the ACP core particle was simulated as a sphere of randomly located calcium ions,

phosphate ions, and water molecules using the Tripos force field and charges from the MMFF94

method (chosen because it gave the correct charge on the phosphate ions). The ACP core particle

was modeled with 144 calcium and 96 phosphate ions and 138 water molecules. The ACP core

particle was energy minimized with full electrostatics and van der Waal's interactions ramped up

from 5% to full value to allow atoms to move past each other to energetically more favourable

locations. The oxygen atoms of the water molecules, as well as the calcium and phosphate ions,

were constrained to be within 12.7 Å of the centre of the ACP core particle. This constraint was

required to prevent destabilization of the ACP core particle in the early stages of the calculation

only, once energy minimized this constraint made no contribution to the total system energy.

For modeling of the β-CN(1-25) residues in the β-CN(1-25)–ACP complex, residues -Val^8-

Pro-Gly-Glu^{11}- were constrained in a β-turn. This was based on nOe observations in the

calcium complex [28], similar chemical shifts for these residues in the calcium and calcium

phosphate complexes, and the known propensity for the sequence motif -Pro-Gly- to occur as

the second and third residues in type-II β-turns. The type-II β-turn was formed by constraining

the ϕ/ψ angles of Pro^9 and Glu^{10} and forcing an H-bond to form between the carbonyl of Val^8

and the amide proton of Glu^{11}.

10

Based on previous modeling studies [43] and specific surface area measurements of CPP bound to HA surfaces [29] further constraints were applied to the polar side-chains of the peptide with the ACP phase. In the early stages of the β-CN(1-25)–ACP modeling process, polar interactions between the peptide and the ACP core were enforced by requiring one oxygen atom of each of the phosphate and carboxylate groups to be in the range 9.0 Å to 16.0 Å from the centre of the ACP particle using a quadratic-well potential with a force constant of 10.1 kcal mole^{-1} Å^{-1}. The interaction between the ACP particle and the guanidino side-chains were enforced by similarly constraining one hydrogen atom from each of the terminal nitrogen atoms to be in the same range from the ACP particle. Since the initial annealing calculations were performed without electrostatics, the role of the ACP particle in these calculations was primarily to enforce proper van der Waal's constraints on the peptides in the calculation. No constraints were applied to the terminal NH_2 or the side-chain of Asn^7.

The model of the β-CN(1-25)–ACP complex was built in several stages. In the first step, the constraints were applied to a single peptide constrained, as described above, to lie on the surface of the ACP sphere. Constraints corresponding to d_{NN} nOes were applied in the form of a quartic-well potential with lower bound distances of 1.8 Å and upper bound distances of 2.7 Å and a force constant of 20 kcal mole^{-1} Å^{-1}. The upper bounds for the Leu^{16}-Pse^{17} and Ser^{22}-Ile^{23} constraints were increased to 4.5 Å because the shorter constraints were systematically violated in the early models. Torsional constraints were implemented with a force constant of 0.06 kcal mole^{-1} degree^{-2}. Simulated annealing was used with the system heated to a temperature of 700 K for 5 ps, and then cooled to 20 K over a period of 2 ps. This cycle was repeated 50 times to generate 50 structures. The twenty lowest energy structures were then taken and individually energy minimized. In the second stage, six peptides identified as (chains

11

A-E) having the lowest energy were arranged around the ACP sphere. The peptides were then

allowed to relax through a molecular dynamics simulation at 300 K for 50 ps, to remove bad

van der Waal's contacts, subject to the constraints previously applied to the single peptide. The

peptide moieties were then fixed and the ACP core was energy minimized, using both

dynamics and energy minimization, while the van der Waal's and electrostatic contributions to

the energy were gradually ramped up to their full values. The peptides were once again energy

minimized subject to the constraints. These calculations were performed using the Tripos force

field with charges calculated by the MMFF94 method.

During the course of the energy minimization, it was noted that water molecules were

escaping from the ACP core and forming H-bonds between the peptide moieties. To ensure that

the H-bonding potential of the peptides were satisfied, the CPP-ACP particle was solvated

using a droplet model with a total of 1239 water molecules. The solvent molecules were

constrained to lie within a sphere of radius 24 Å from the nanocomplex centre by a quartic-well

potential with a force constant of 7 kcal mole^{-1} Å^{-1} to prevent evaporation of solvent molecules.

The energy minimization was carried out using the full MMFF94s force field including

electrostatic interactions and a dielectric constant of unity. Energy minimization was continued

until the average force on the atoms fell below 0.05 kcal mole^{-1} Å^{-1}.

To ensure that the energy-minimized structure was not trapped in a local minimum, a 60 ps

dynamics simulation at 300 K was performed with a dynamics step size of 0.75 fs. Three

conformations having low potential energy were selected at 8.910 ps, 40.068 ps, and 56.028 ps

respectively, and energy minimized until the average force on the atoms fell below 0.05 kcal

mole^{-1} Å^{-1}. To confirm that the peptide constraints were not distorting the final structures the

12

force constants for torsional constraints and nOe distance constraints were set to zero and the

structure from the third model was energy minimized for a further 100 iterations.

The program NMRCLUST [44] was used to investigate the conformational properties of the

β-casein(1-25) peptides bound to the ACP core particle. Secondary structural features of the

peptides conformations were identified using STRIDE [45].

RESULTS

Electrophoresis of cross-linked α_{S1}-CN(59-79). Incubation of α_{S1}-CN(59-79) with

glutaraldehyde in the presence of either calcium alone or calcium and phosphate resulted in the

cross-linking of the α_{S1}-CN(59-79) peptides. Fig. 1 shows the migration of glutaraldehyde cross-

linked α_{S1}-CN(59-79) in a 20% native gel. In the absence of calcium, or in the presence of

phosphate only (not shown), the largest aggregate observed was a dimer. In the presence of

either calcium or calcium phosphate, the largest multimer observed was a hexamer.

NMR Spectroscopy Studies β-CN(1-25)–ACP. The decay of the echo amplitude due to

translational diffusion of β-CN(1-25)–ACP complex was measured using the sLED technique [38].

At a concentration of 1.0 mM β-CN(1-25), the decay of the echo amplitude was single

exponential (Fig. 2). The Stokes-Einstein equation, [2], relating the translational diffusion

coefficient, the hydrodynamic radius, the sample viscosity, and the temperature was used to

estimate the relative sizes of water molecules (hydrodynamic radius ~1.40 Å) and the complexes.

13

The hydrodynamic radius of the carrier particles was most accurately determined by the experiments recorded with a diffusion delay, Δ, of 200 ms due to the greater dynamic range for this experiment. The behaviour of the signals recorded at shorter diffusion delay times were consistent with the value determined at the longer diffusion delay time. An estimated hydrodynamic radius of 1.526 ± 0.044 nm was determined for the β-CN(1-25)–ACP complex at pH 6.0 increasing to 1.923 ± 0.082 nm at pH 9.0. The degeneracy of the HDO resonance and the Hα resonance of Asn[7] resulted in a bi-exponential decay of the calibration resonance even at the lower sample concentration and was responsible for much of the error associated with the estimate of the hydrodynamic radius. At a higher concentration of 4.5 mM β-CN(1-25), the decay of the echo amplitude was multi-exponential (Fig. 2b) indicating aggregation of the complexes.

The CLEANEX-PM [39] experiment was used to identify the solvent exposed protons of the peptide moieties in the β-CN(1-25)–ACP complex by transfer of magnetization from the solvent water to the peptide. The only resonances observed in this experiment were in the Hα region and were assigned to the Hδ protons of Pro[9], the Hα proton of Val[8], the Hα proton of either Ile[12] or Val[13] or possible both, and a glutamate Hα proton (Fig. 3). The signals were observed to increase in intensity as the mixing period increased from 50 ms to 300 ms in 50 ms steps (Fig. 3) ruling out an artifactual response.

One and Two-dimensional NMR Spectroscopy of β-CN(1-25)–ACP. In contrast to the spectra of β-CN(1-25) complexed with calcium alone[28], the NMR spectra of β-CN(1-25)–ACP were markedly sharper with well-resolved $^3J_{H^N-H^\alpha}$ splittings observed in the amide region (Fig. 4). The

14

amide resonances were well dispersed. The measured $^3J_H{}^N\text{-}_H{}^\alpha$ ranged from a low of 5.5 Hz to a high of 8.1 Hz with no significant tendency for runs of low or high values to occur in adjacent residues. The observation of $^3J_H{}^N\text{-}_H{}^\alpha$ coupling constants that differed significantly from the random-coil value of about 6 to 7 Hz clearly indicated that the peptide adopts a preferred conformation when bound to the ACP phase.

Analysis of the line widths indicated that they were similar for all residues and hence the dynamics of residues were similar. Furthermore there was no evidence for particular residues having markedly different dynamics from neighbouring residues due to interactions with the calcium phosphate core particles. The resonances of the phosphoseryl residues could be readily assigned from TOCSY and NOESY spectra. Sequential d_{NN} and $d_{\alpha N}$ nOes were observed allowing the spectra to be sequentially assigned. Table 1 summarized the coupling constants and the ^1H NMR assignments obtained.

A number of NOESY spectra were acquired with mixing times up to 250 ms. Fig. 5 shows the finger print region and the amide region of a NOESY spectrum acquired with a mixing time of 250 ms. All NOESY cross-peaks were explicable as intramolecular cross-peaks. Since no signals were observed in spectra acquired at 300 ms, this absence of medium- and long-range intramolecular nOes indicated that the peptides adopted an extended conformation. The observed nOes and $^3J_H{}^N\text{-}_H{}^\alpha$ coupling constants, summarized in Fig. 6, were used to build a model of the peptide in the β-casein(1-25)–ACP nanocomplex.

Molecular modeling of the β-casein(1-25)–ACP nanocomplex. The model was built in several stages. At the first step, each peptide was assigned a unique chain label A-E. This was used to follow the progress of the chains during the dynamics runs. Three molecular models of the β-

15

CN(1-25)-ACP nanocomplex were constructed. In the final dynamics run the first was annealed

for 8.910 ps, the second for 40.068 ps, and the third for 56.028 ps prior to energy minimization.

The models of the β-CN(1-25)-ACP nanocomplex are both chemically and stereochemically

reasonable as can be seen from the statistics presented in Table 2. Inspection of the

Ramachandran plot, for the third model, shows that the majority of the ϕ/ψ angles are in either

the 'core' or 'allowed' regions and that only a few residues are in the 'forbidden' region: Glu^5

with four examples in the 'forbidden' region is particularly noteworthy. All models satisfy the

NMR torsion constraints, while the NMR distance constraints are reasonably well satisfied with no

pattern of systematic violations. The peptide backbones of model 3 and the structure resulting

from the unrestrained minimization could be superimposed with an RMSD of 0.226 Å, confirming

that the NMR constraints were not significantly distorting the peptide conformation.

Analysis of the peptide secondary structure in model 3 using STRIDE [45] showed that the

peptides (chains A-E) adopt secondary structures consisting of a series of β-turns. Type IV β-

turns were identified for Glu^4-Asn^7 and $Ser(P)^{19}$-Ser^{22} in all chains, a type VIII β-turn was

identified for Glu^{14}-$Ser(P)^{17}$ in all chains except B and E, and a type IV β-turn was identified for

Leu^3-Leu^6 in chains B, E, and F. The region from Val^8 to Ile^{12} does not adopt a single

conformation across the different chains: the A-chain has a type II β-turn for Val^8-Glu^{11}, a type

IV β-turn for Pro^9-Ile^{12} followed by a type VIII β-turn for Glu^{11}-Glu^{14}, in chains B, D, and E

there is a type IV β-turn for Val^8-Glu^{11}, in chain F a short 3_{10}-helix connects Pro^9-Glu^{11}, while in

chain C no secondary structure assignment was made.

Fig. 7 shows the model of β-CN(1-25)–ACP based on the constraints previously summarized

in Fig. 6. The model consists of an ACP core of radius 1.27 nm consisting of 96 phosphate ions,

16

144 calcium ions and 132 water molecules (six water molecules escaped from the core during modeling). This core is surrounded by six β-CN(1-25) peptides. Binding energies were calculated by ignoring the solvent molecules, using a distance-dependent dielectric of r/2, and an electrostatic cutoff distance of 8 Å. The structure is predicted to be stable with a net average binding energy of −1265 kcal/(mole of peptide). The average interaction between the ACP core and the peptides was −1270 ± 430 kcal/(mole of peptide). The peptide-peptide interactions were overall repulsive with an average value of 54 ± 210 kcal/(mole of peptide). However in solution, these repulsive interactions would be shielded by the polar solvent and counter ions. It is probable that individual peptide chains can be inserted with random orientations into the β-CN(1-25)–ACP nanocomplex since the packing of peptides was determined by strong, electrostatic peptide–ACP interactions rather than the weaker, van der Waal's peptide-peptide interactions.

The model was subjected to a series of analyses. The interface was defined as the set of atoms that belong to either the ACP core or the peptides that were within 2.5 Å of atoms belonging to the peptides or the core respectively. Analysis of the interface revealed that each peptide contributed, on average, 41 atoms to the interface forming contacts with a similar number of core atoms. These atoms interacted through either electrostatic or H-bonding that make a considerable contribution to the overall stability of the complex as modeled. Four of the six unconstrained side-chains of Asn[7] formed H-bonds with core atoms, while in three of the peptides, an H-bond was formed between the terminal amide of Arg[1] to the carbonyl oxygen of the Asn[7] side-chain. In all cases where there was an electrostatic interaction between an oxygen atom and a calcium ion from the core, the oxygen atoms were associated with either the side-chains or the C-terminal

carboxyl group; the backbone carbonyl groups did not form part of the interface. Fig. 8 shows

one of the peptides and the atoms of the ACP core within 2.5 Å of the peptide.

The conformations of individual peptides within the models were also analysed.

Superimposing the heavy backbone atoms of the peptides from any of the models showed that

the peptide adopts a reasonably well-defined conformation. The root mean squared deviation of

the backbone atoms of the peptides of the third model from their average position was 2.149 Å.

However, when the conformations of the peptides from all three models were compared and

clustered (using NMRCLUST[44]) a total of six conformational clusters were found with backbone

RMSDs ranging from 0.578 Å to 0.846 Å. Each cluster consisting of the corresponding peptide

chains from the each of the three models: that is the three A chains form one cluster, the three B

chains another, and so on. The modeling suggested that the peptide adopted a conformation close

to the ensemble average conformation but with minor changes to better accommodate differences

in the mineral surface with which the peptide is interacting. This interpretation of the modeling

result is supported by the observation that when the heavy atoms of the peptides are

superimposed, the polar residues make the largest contributions to the calculated heavy-atom

RMSD. Of the thirteen residues that make an above average contribution to the calculated heavy-

atom RMSD only Ile^{23} is non-polar. Furthermore the only polar residues that make below average

contributions to the heavy-atom RMSD are Asn^7, Glu^{20}, Ser^{22}, and Thr^{24} (predominantly the

neutral, polar residues). This is consistent with the charged, polar residues making specific

interactions with features of the ACP core that vary with the location of one peptide chain to that

of another.

Analysis of the residues that contributed most to the RMSD of the backbone atoms from the

average conformation revealed that the residue that deviated most was Gly^{10}. Residue Gly^{10}

18

showed ϕ/ψ isomerism with two populations having approximate ϕ/ψ angles of 100º/30º and -

100º/-75º respectively. This was observed despite the use of constraints on the ϕ/ψ angle of this

residue to force a β-turn between Val[8] and Glu[11]. Inspection of two representative chains

indicated that both structures contain a similar set of H-bonds that served to stabilize a β-turn

with different backbone conformations at Gly[10]. Further scrutiny of the STRIDE[45] analysis of

model 3, revealed a variety of secondary structural features for Val[8] to Glu[11] consistent with this

region of the peptide backbone having some flexibility.

The intrapeptide, proton-proton distances from the models were measured to account for the

absence of non-sequential nOes in the ^{1}H NMR spectra. For example, the distance from Leu[3] Hα

to Val[8] Hβ ranged from 2.726 Å to 9.927 Å in the peptides of model 3. After taking into account

the R[-6] dependence of the nOe on the interatomic distance, averaging over the six peptides in

model 3 yielded an effective distance of 3.67 Å for these two protons. A nOe that is readily

observed between two atoms at 2.726 Å would be much harder to observe at the longer average

distance. Calculations using intrapeptide, proton-proton distances from model 3 confirmed that

the distance dependence of the nOe effect biases against the observation of non-sequential nOes

relative to the observed sequential nOes. Consequently, the absence of non-sequential nOes in

the ^{1}H NMR spectra is consistent with the ability of the β-casein(1-25) peptide to adapt to

differences in the mineral surface.

DISCUSSION

19

NMR spectroscopy reveals differences between the structures of β-CN(1-25) complexed with calcium and with ACP. In contrast to previous studies[46], all residues in the complexes of β-CN(1-25)–ACP were assigned. Previously the Hα resonances of the phosphoseryl residues were reported to be not observable based on the inspection of one-dimensional spectra of β-CN(1-25)–ACP, with the explanation they had been broadened due to their rigid attachment to the slowly tumbling amorphous calcium phosphate core particle. However in the calcium ion complexes, these resonances have higher frequencies than the other Hα protons, and the resonances are observable in a narrow window between the water resonance and the other Hα resonances. Our assignment of the two-dimensional spectra in the current study shows that in the complex with calcium phosphate, these resonances move to significantly lower frequencies and the resonances now overlap the Hα resonances of the other residues.

In contrast to the spectra of β-CN(1-25) complexed with calcium alone[28], the NMR spectra of β-CN(1-25)–ACP revealed only nOes corresponding to sequential d_{NN}, $d_{\alpha N}$, and $d_{\beta N}$ connectivities. No NOESY cross-peaks were observed at longer mixing times, that is for mixing times of 300 ms or greater, including the intraresidue and sequential cross-peaks noted at shorter mixing times. This observation suggests that relaxation of the nuclear spins by the spin-diffusion mechanism is efficient. The absence of medium- and long-range nOes might be explained if the long-range neighbouring protons were disordered, the amplitude of the many possibly medium- and long-range nOes from a particular proton falling below the threshold required for observation. This is consistent with a model of the CPP–ACP particle in which strong peptide-ACP interactions (i.e. electrostatic) are responsible for holding the complex together. The weaker, non-specific peptide-peptide interactions (i.e. van der Waal's forces) allow the peptides to be packed, but do not force the peptides into a specific regular arrangement.

20

The CPP-ACP complexes pose experimental challenges during the acquisition of structural data. One of the key features of the CPP–ACP complexes is the ease with which large aggregates form. Due to aggregation we have noted that solutions form clear, thixotropic gels at sufficiently high complex concentrations. We have used a wide variety of techniques in an approach to determine particle sizes for these complexes. Even simple techniques such as the use of microfilters with a known pore size can give contradictory results, as CPP–ACP at low concentrations move freely through 0.2 μm filters but are retained at higher concentrations. We have applied a variety of light-scattering techniques to CPP-ACP solutions and have obtained characteristic dimensions ranging from 3-300 nm. These experiments are not discussed in detail because we believe the results relate to aggregates; however, they do emphasize the need to ensure that measurements relate to the monomeric species. Hence, a structural model of the β-CN(1-25)–ACP complex provides insight into the architecture of the CPP-ACP complex incorporating several different peptides.

The β-CN(1-25)–ACP nanocomplex model is consistent with a range of experimental observations. In attempting to model the β-CN(1-25)–ACP complex, it was necessary to satisfy a number of constraints from a wide variety of experimental sources. Some of the constraints, for example the distance and torsion constraints from the NMR experiments, were used directly to provide numeric constraints on the peptides in our model. Other constraints, for example the size of the complex and the number of calcium and phosphate ions bound per peptide, were incorporated into our model. Finally, there were a number of experimental observations, for example, the rheological behaviour of concentrated solutions of the β-CN(1-25)–ACP complex

21

that cannot be used to constrain the modeling, but should be explicable in terms of features of the final model.

Glutaraldehyde cross-linking of the peptides in the α_{S1}-CN(59-79)–ACP complex suggested that up to six peptides are involved in the formation of each nanocomplex. We have assumed that the β-CN(1-25)–ACP complex has a similar structure. Specific surface area, binding data, and hydrodynamic radius measurements are consistent with this assumption[29].

We have very little information about the ACP core. Our chemical binding studies indicated that there are a maximum of 14 and 16 phosphate ions in the complexes formed by α_{S1}-CN(59-79) and β-CN(1-25) respectively[30]. Hence assuming there are six peptides per complex then there are a maximum of 96 phosphate ions per β-CN(1-25)–ACP complex. For simplicity, the ACP is treated as having the composition $Ca_3(PO_4)_2$. The actual non-stoichiometric composition[32] implies an additional 5 calcium ions and associated hydroxyl ions for the β-CN(1-25)–ACP complex. In addition to these known components of the ACP core, there is evidence, from the behaviour of CPP–ACP under heat treatment at or slightly above 100 °C, that there is water in the calcium phosphate phase. Heat treatment tends to produce material with less bio-available calcium and phosphate and X-ray powder diffraction patterns indicating some partial crystallinity with conversion to a disordered apatitic phase [32]. We have chosen to model the ACP core with 138 water molecules, however, the dimensions of the core particle were not very sensitive to the number of water molecules included in the model. The predicted radius of the ACP core is then about 1.27 nm, in good agreement with the electron microscopy observations of ACP from casein micelles[9, 47].

Two observations suggest that the ACP core particles in milk are coated by the caseins and that the caseins do not form an integral part of the ACP core. First, the caseins can be removed

22

by chemical treatments such as soaking in a solution of hydrazine[9, 47]. Second, the CLEANEX-PM experiment reported above, indicated that some protons are solvent exposed. These observations are consistent with the protein not being embedded in the mineral phase.

The calcium phosphate binding studies performed with the CPP and analogues revealed a strong correlation between peptide length and the number of bound calcium and phosphate ions[32]. This observation suggests that the entire length of the peptides is involved in interactions with the amorphous calcium phosphate phase, not just the 'calcium-binding motif' -(Ser(*P*)-)$_3$(Glu-)$_2$. This is consistent with the highly polar nature of the CPP peptides, which contain many negatively charged residues such as glutamyl and phosphoseryl residues outside of the so-called 'calcium-binding motif'.

The calculated dimensions of the β-CN(1-25)–ACP are consistent also with the previously unexplained observation of a secondary maximum in the X-ray and neutron diffraction studies at a scattering vector of $Q \sim 1.6$ nm^{-1} [48].

Our model of the CPP–ACP complex is fundamentally different from that proposed by Holt *et al.* [48]. The values derived by Holt *et al.* [48] suggest an ACP core with a radius of about 2.30 nm coated by 48 peptides. The thickness of the peptide coat, 17.4 Å, implies that each peptide occupies a volume of about 4.69 nm^3, compared to a van der Waal's volume of about 1.06 nm^3 for the β-CN(1-25) peptide. The peptide chains can only fill this volume if a substantial proportion of each peptide is in rapid motion forming an 'entropic brush' [49]. Such a description is inconsistent with the authors' own description of the peptide coat as being dense. Furthermore, it is unclear why such a polar peptide should be in rapid motion when attached to a highly polar calcium phosphate surface.

23

The model of the β-CN(1-25)–ACP complex also provides some insight into the rheological behaviour of the complexes. A large, hydrophobic patch on the surface of the complex is revealed in the model. This patch contains Pro^9, Ile^{12}, Val^{13} and a glutamate residue, Glu^5. These residues were not constrained by our modeling procedure, and the prediction that these residues should be solvent exposed is consistent with the CLEANEX-PM experimental results. Hydrophobic interactions between patches on different complexes would be predicted to mediate the aggregation of these complexes: this prediction is consistent with the observed solution behaviour of these complexes.

The observation of ϕ/ψ isomerism at Gly^{10} may explain the doubling of the ^1H NMR transitions that was previously ascribed to *cis/trans* isomerism of Pro^9 in the β-casein(1-25) calcium complex [28, 50, 51].

CONCLUSIONS

The ability of glutaraldehyde to cross-link up to six α_{S1}-CN(59-79) molecules in the presence of either calcium ions alone or calcium and phosphate ions, combined with earlier results [32] suggests a nanocomplex having the formula $[\alpha_{S1}$-CN(59-79)-(ACP)$_7]_6$. The corresponding β-CN(1-25)–ACP nanocomplex has the formula $[\beta$-CN(1-25)-(ACP)$_8]_6$.

A molecular model of the β-CN(1-25)–ACP nanocomplex based on NMR observations combined with a variety of earlier results suggests that the dominant interactions within the complex are between the ACP core and the peptides with weaker interactions between the peptides. The model demonstrates chemically reasonable interactions between the ACP core and the peptides and is consistent with a wide variety of experimental observations. The model predicts the occurrence of 'patches' containing lipophilic residues at the surface of the

24

nanocomplex, these patches may account for the observed tendency toward aggregation of the

nanocomplexes. Because such lipophilic patches would allow interactions between the

nanocomplexes and biological membranes, this feature may play an important role in the

biological function of these peptides as biological delivery vehicles for calcium and phosphate.

ACKNOWLEDGMENTS

25

REFERENCES

(1)   Walstra, P., and Jenness, R. (1984) *Dairy chemistry and physics*, John Wiley and Sons,

New York, N.Y.

(2)   Van Hooydonk, A. C. M., Boerrigter, I. J., and Hagedoorn, H. G. (1986) pH-induced

physicochemical changes of casein micelles in milk and their effect on renneting. 2.

Effect of pH on renneting of milk, *Neth. Milk Dairy J. 40*, 297-313.

(3)   Holt, C., and Sawyer, L. (1988) Primary and predicted secondary structures of the caseins

in relation to their biological functions, *Protein Eng. 2*, 251-259.

(4)   Dalgleish, D. G., and Corredig, M. (2012) The structure of the casein micelle of milk and

its changes during processing, *Annu Rev Food Sci Technol 3*, 449-467.

(5)   Holt, C., Carver, J. A., Ecroyd, H., and Thorn, D. C. (2013) Invited review: Caseins and

the casein micelle: their biological functions, structures, and behavior in foods, *J. Dairy

Sci. 96*, 6127-6146.

(6)   Ingham, B., Erlangga, G. D., Smialowska, A., Kirby, N. M., Wang, C., Matia-Merino, L.,

Haverkamp, R. G., and Carr, A. J. (2015) Solving the mystery of the internal structure of

casein micelles, *Soft Matter 11*, 2723-2725.

(7)   Tercinier, L., Ye, A., Anema, S. G., Singh, A., and Singh, H. (2014) Interactions of

casein micelles with calcium phosphate particles, *J Agric Food Chem 62*, 5983-5992.

(8)   Schmidt, D. G. (1982) Association of caseins and casein micelle structure., *Dev. Dairy

Chem. 1*, 61-86.

26

(9) McGann, T. C., Buchheim, W., Kearney, R. D., and Richardson, T. (1983) Composition and ultrastructure of calcium phosphate-citrate complexes in bovine milk systems, *Biochim. Biophys. Acta 760*, 415-420.

(10) de Kruif, C. G. (1999) Casein micelle interactions, *Int. Dairy J. 9*, 183-188.

(11) Holt, C., and Horne, D. S. (1996) The hairy casein micelle: evolution of the concept and its implications for dairy technology, *Neth. Milk Dairy J. 50*, 85-111.

(12) Reynolds, E. C., Black, C. L., Cai, F., Cross, K. J., Eakins, D., Huq, N. L., Morgan, M. V., Nowicki, A., Perich, J. W., Riley, P. F., Shen, P., Talbo, G., and Webber, F. (1999) Advances in enamel remineralization: casein phosphopeptide-amorphous calcium phosphate, *J. Clin. Dent. 10*, 86-88.

(13) Adamson, N. J., Riley, P. F., and Reynolds, E. C. (1993) The analysis of multiple phosphoseryl-containing casein peptides using capillary zone electrophoresis., *J. Chromatogr. 646*, 391-396.

(14) Reynolds, E. C., Riley, P. F., and Adamson, N. J. (1994) A selective precipitation procedure for the purification of multiple-phosphoseryl containing peptides and their identification., *Anal. Biochem. 217*, 277-284.

(15) Reynolds, E. C., Cain, C. J., Webber, F. L., Black, C. L., Riley, P. F., Johnson, I. H., and Perich, J. W. (1995) Anticariogenicity of calcium phosphate complexes of tryptic casein phosphopeptides in the rat, *J. Dent. Res. 74*, 1272-1279.

(16) Reeves, R. E., and Latour, N. (1958) Calcium phosphate sequestering phosphopeptide from casein., *Science 128*, 472.

(17) Mykkanen, H. M., and Wasserman, R. H. (1980) Enhanced absorption of calcium by casein phosphopeptides in rachitic and normal chicks., *J. Nutr. 110*, 2141-2148.

27

(18)   Lee, S. L., and Veis, A. (1980) Cooperativity in calcium ion binding to repetitive,

carboxylate-serylphosphate polypeptides and the relationship of this property to dentin

mineralization, *Int. J. Pept. Protein Res. 16*, 231-232.

(19)   Lee, Y. S., Noguchi, T., and Naito, H. (1983) Intestinal absorption of calcium in rats

given diets containing casein or amino acid mixture: the role of casein phosphopeptides,

Br. J. Nutr. 49, 67-76.

(20)   Sato, R., Noguchi, T., and Naito, H. (1986) Casein phosphopeptide (CPP) enhances

calcium absorption from the ligated segment of rat small intestine, *J. Nutr. Sci. Vitaminol.
32*, 67-76.

(21)   Meisel, H., and Fristar, H. (1988) Chemical characterization of a caseinophosphopeptide

isolated from *in vivo* digests of a casein diet., *Biol. Chem. Hoppe Seyler 369*, 1275-1279.

(22)   Gerber, H. W., and Jost, R. (1986) Casein phosphopeptides: their effect on calcification

of in vitro cultured embryonic rat bone., *Calcif. Tiss. Int 38*, 350-357.

(23)   Reynolds, E. C. (1991) Anticariogenic phosphopeptides. United States Patent 5,015,628.

(24)   Shen, P., Cai, F., Nowicki, A., Vincent, J., and Reynolds, E. C. (2001) Remineralization

of enamel subsurface lesions by sugar-free chewing gum containing casein

phosphopeptide-amorphous calcium phosphate, *J. Dent. Res. 80*, 2066-2070.

(25)   Reynolds, E. C., Cai, F., Shen, P., and Walker, G. D. (2003) Retention in plaque and

remineralization of enamel lesions by various forms, *J. Dent. Res. 82*, 206-211.

(26)   Kitts, D. D., Yuan, Y. V., Nagasawa, T., and Moriyama, Y. (1992) Effect of casein,

casein phosphopeptides and calcium intake on ileal 45Ca disappearance and temporal

systolic blood pressure in spontaneously hypertensive rats, *Br. J. Nutr. 68*, 765-781.

(27)   Ferraretto, A., Signorile, A., Gravaghi, C., Fiorilli, A., and Tettamanti, G. (2001) Casein

phosphopeptides influence calcium uptake by cultured human intestinal HT-29 tumor

cells, *J. Nutr. 131*, 1655-1661.

(28)   Cross, K. J., Huq, N. L., Bicknell, W., and Reynolds, E. C. (2001) Cation-dependent

structural features of beta-casein-(1-25), *Biochem. J. 356*, 277-286.

(29)   Cross, K. J., Huq, N. L., O'Brien-Simpson, N. M., Perich, J. W., Attard, T. J., and

Reynolds, E. C. (2007) The role of multiphosphorylated peptides in mineralized tissue

regeneration, *Int. J. Pept. Res. Ther. 13*, 479-495.

(30)   Cross, K. J., Huq, N. L., Palamara, J. E., Perich, J. W., and Reynolds, E. C. (2005)

Physicochemical characterization of casein phosphopeptide-amorphous calcium

phosphate nanocomplexes, *J. Biol. Chem. 280*, 15362-15369.

(31)   Cross, K. J., Huq, N. L., Stanton, D., Sum, M., and Reynolds, E. C. (2003) NMR

spectroscopy and mass spectrometry studies of a novel calcium, phosphate and fluoride

delivery vehicle - the multiphosphorylated peptide alpha(SI)-Casein(59-79) complexed

with amorphous calcium fluoride phosphate, *J. Dent. Res. 82*, 92.

(32)   Cross, K. J., Huq, N. L., Stanton, D. P., Sum, M., and Reynolds, E. C. (2004) NMR

studies of a novel calcium, phosphate and fluoride delivery vehicle - α_{S1}-Casein(59-79)

complexed with amorphous calcium fluoride phosphate, *Biomaterials 25*, 5061-5069.

(33)   Huq, N. L., Cross, K. J., and Reynolds, E. C. (1995) A ^{1}H NMR Study of the casein

phosphopeptide α_{S1}-Casein(59-79), *Biochim. Biophys. Acta 1247*, 201-208.

(34)   Huq, N. L., Cross, K. J., and Reynolds, E. C. (2003) Nascent helix in the

multiphosphorylated peptide alphaS2-casein(2-20), *J. Pept. Sci. 9*, 386-392.

29

(35)   Davis, B. J. (1964) Disc electrophoresis. II. Method and application to human serum

proteins, *Ann. N. Y. Acad. Sci. 121*, 404-427.

(36)   Green, M. R., Pastewska, J. V., and Peacock, A. C. (1973) Differential staining of

phosphoproteins on polyacrylamide gels with a cationic carbo-cyanine dye, *Anal.*

Biochem. 56, 43-51.

(37)   Reynolds, E. C. (2013) Stabilized calcium phosphate complexes. United States Patent

8,609,071.

(38)   Altieri, A. S., Hinton, D. P., and Byrd, R. A. (1995) Association of biomolecular systems

via pulsed field gradient NMR self-diffusion measurements., *J. Am. Chem. Soc. 117*,

7566-7567.

(39)   Hwang, T. L., Mori, S., Shaka, A. J., and Vanzijl, P. C. M. (1997) Application of phase-

modulated clean chemical exchange spectroscopy (cleanex-pm) to detect water-protein

proton exchange and intermolecular noes, *J. Am. Chem. Soc. 119*, 6203-6204.

(40)   States, D. J., Haberkorn, R. A., and Ruben, D. J. (1982) A two-dimensional nuclear

Overhauser experiment with pure absorption phase in four quadrants, *J. Magn. Reson. 48*,

286-292.

(41)   Wüthrich, K. (1986) *NMR of Proteins and Nucleic Acids*, Wiley and Sons, New York.

(42)   Chazin, W. J., and Wright, P. E. (1987) A modified strategy for identification of ^{1}H spin

systems in proteins., *Biopolymers 29*, 973-977.

(43)   Huq, N. L., Cross, K. J., and Reynolds, E. C. (2000) Molecular modelling of a multi-

phosphorylated sequence motif bound to hydroxyapatite surfaces, *J. Mol. Model. 6*, 35-

47.

30

(44)   Kelley, L. A., Gardner, P. G., and Sutcliffe, M. J. (1996) An automated approach for

         clustering an ensemble of NMR-derived protein structures into conformationally-related

         subfamilies., *Protein Eng. 9*, 1063-1065.

(45)   Frishman, D., and Argos, P. (1995) Knowledge-based protein secondary structure

         assignment, *Proteins: Struct., Funct., Genet. 23*, 566-579.

(46)   Holt, C., Wahlgren, N. M., and Drakenberg, T. (1996) Ability of a beta-casein

         phosphopeptide to modulate the precipitation of calcium phosphate by forming

         amorphous dicalcium phosphate nanoclusters, *Biochem. J. 314*, 1035-1039.

(47)   McGann, T. C., Kearney, R. D., Buchheim, W., Posner, A. S., Betts, F., and Blumenthal,

         N. C. (1983) Amorphous calcium phosphate in casein micelles of bovine milk, *Calcif.*

         Tiss. Int 35, 821-833.

(48)   Holt, C., Timmins, P. A., Errington, N., and Leaver, J. (1998) A core-shell model of

         calcium phosphate nanoclusters stabilized by beta-casein phosphopeptides, derived from

         sedimentation equilibrium and small-angle x-ray and neutron-scattering measurements,

         Eur. J. Biochem. 252, 73-78.

(49)   Bright, J. N., Woolf, T. B., and Hoh, J. H. (2001) Predicting properties of intrinsically

         unstructured proteins, *Prog. Biophys. Mol. Biol. 76*, 131-173.

(50)   Tsuda, S., Niki, R., Kuwata, T., Tanaka, I., and Hikichi, K. (1991) Proton NMR study of

         casein phosphopeptide (1-25): Assignment and conformation, *Magn. Reson. Chem. 28*,

         1097-1102.

(51)   Wahlgren, N. M., Léonil, J., Dejmek, P., and Drakenberg, T. (1993) Two-dimensional

         nuclear magnetic resonance study of the β-casein peptide 1-25: Resonance assignments

         and secondary structure., *Biochim. Biophys. Acta 1202*, 121-128.

31

(52) Cornell, W. D., Cieplak, P., Bayly, C. I., Gould, I. R., Merz, K. M., Jr., Ferguson, D. M.,

Spellmeyer, D. C., Fox, T., Caldwell, J. W., and Kollman, P. A. (1995) A second

generation force field for the simulation of proteins, nucleic acids, and organic

molecules., *J. Am. Chem. Soc. 117*, 5179-5197.

Table 1: $^3J_H{}^N\text{-}_H{}^\alpha$ coupling constants and proton chemical shifts for β-casein(1-25) – ACP nanocomplex at 25º C and pH 6.00.

Residue	$^3J_H{}^N\text{-}_H{}^\alpha$	NH	Hβ	Hβ	Hγ	Hδ	γCH$_3$	NH$_2$
Arg^1	-	-	4.01	1.89, 1.89	1.65, 1.65	3.23, 3.23		
Glu^2	6.2	8.62	4.23	1.95, 1.95	2.26, 2.26			
Leu^3		8.48	4.25	1.62, 1.62	1.62	0.90, 0.90		
Glu^4		8.45	4.24	1.96, 1.96	2.24, 2.24			
Glu^5		8.51	4.29	1.95, 1.95	2.22, 2.22			
Leu^6	6.6	8.25	4.35	1.59, 1.59	1.59	0.88, 0.88		
Asn^7		8.44	4.60	2.70, 2.79				
Val^8	8.1	8.15	4.40	2.06	0.92, 0.92			
Pro^9	-	-	4.44	2.32, 2.29	2.01, 1.96	3.87, 3.71		
Gly^{10}		8.40	4.00, 3.87					
Glu^{11}		8.19	4.28	1.91, 1.91	2.21, 2.21			
Ile^{12}	8.1	8.31	4.17	1.82	1.47, 1.17	0.84	0.84	
Val^{13}		8.36	4.15	-	0.90, 0.90			
Glu^{14}	7.0	8.53	4.34	2.02, 1.91	2.24, 2.24			
Pse^{15}	6.2	8.69	4.53	4.03, 4.03				
Leu^{16}		8.44	4.47	1.62, 1.62	1.62	0.88, 0.88		
Pse^{17}	6.2	8.72	4.59	4.12, 4.12				
Pse^{18}	5.9	8.79	4.61	4.12, 4.12				
Pse^{19}	5.5	8.76	4.54	4.12, 4.12				
Glu^{20}		8.37	4.27	2.01, 2.01	2.29, 2.29			
Glu^{21}		8.41	4.25	2.01, 2.01	2.27, 2.27			

33

Ser[22]		8.37	4.44	3.86, 3.86			
Ile[23]	7.7	8.09	4.26	1.90	1.45, 1.19	0.89	0.89
Thr[24]	7.3	8.24	4.33	4.18	1.19		
Arg[25]	7.7	8.00	4.18	1.83, 1.72	1.58, 1.58	3.16, 3.16	7.22

34

Table 2: Summary of local geometric properties and NMR constraints for the β-casein(1-25) – ACP model.

Model Property	Value	RMSD
Bond lengths	Tabulated.[52]	±0.017 Å
Bond angles	Tabulated. [52]	±3.02º
Peptide linkages	180º	±11.5º
NMR range constraints	See text.	±0.22 Å
NMR torsion constraints	See text.	±2.95º

35

FIGURE LEGENDS

Figure 1: Native gel showing the migration of α_{S1}-CN(59-79) complexed with calcium and then cross-linked with glutaraldehyde. Lane (a) α_{S1}-CN(59-79) alone, lane (b) α_{S1}-CN(59-79) complexed with calcium ions, and lane (c) α_{S1}-CN(59-79) complexed with calcium and phosphate ions.

Figure 2: Representative sLED data, the signals are integrals over the methyl resonances, for the β-CN(1-25)–ACP complex. The solid curve and associated data points are from a sample having a peptide concentration of 1.0 mM, the solid curve represents the fit to equation [3]. The dashed curve represents the fit to the first six data points acquired for a sample having a peptide concentration of 4.5 mM, note the deviation between the experiment and theory at higher gradient strengths indicative of the formation of aggregates.

Figure 3: CLEANEX-PM spectrum of β-CN(1-25)–ACP complex showing resonances of solvent exposed Hα protons of Val^8, Ile^{12} or Val^{13}, and a glutamate residue, and the solvent exposed Hδ proton of Pro^9.

Figure 4: Comparison of amide spectral regions of [A] β-casein(1-25) calcium ion complex, and [B] β-casein(1-25) – ACP nanocomplex.

36

Figure 5: (A): Amide region of NOESY recorded with a mixing time of 250 ms of the

β-CN(1-25)–ACP complex showing sequential d_{NN} nOe connectivities, (B) finger-print

region from same NOESY spectrum.

Figure 6: Diagrammatic summary of observed nOes and $^{3}J_{H}^{N}{-}_{H}^{\alpha}$ couplings in the

β-CN(1-25)–ACP complex.

Figure 7: Model of β-CN(1-25)–ACP complex using constraints summarized in the text:

(A) the ACP core is shown as CPK space-filling atoms while the peptide backbones are

shown in ribbon form. Each chain is '*rainbow*' *colour* coded with shades of red toward the

C terminus. (B) the Connelly solvent accessible surface of one of the peptides has been

coloured by the hydrophilicity of the peptide and the residues associated with hydrophobic

regions are labeled.

Figure 8: Detail of the β-CN(1-25)–ACP complex showing one of the peptides and the core

atoms forming the interface with the peptide. Interface core atoms are shown as colour-

coded spheres: oxygen atoms are red; calcium atoms are orange; and hydrogen atoms are

teal. Polar contacts at 2.5 Å or less are identified by blue, dashed lines and all contacts at
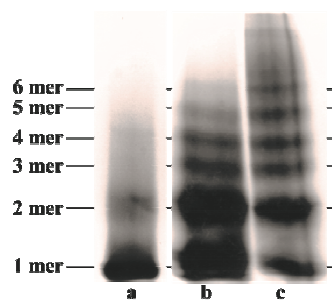
3.0 Å or less by green, dashed lines.

FIGURE 1

1
2
3
4
5
6
7
8
9
10
11
12
13
14
15
16
17
18
19
20
21
22
23
24
25
26
27
28
29
30
31
32
33
34
35
36
37
38
39
40
41
42
43
44
45
46
47
48
49
50
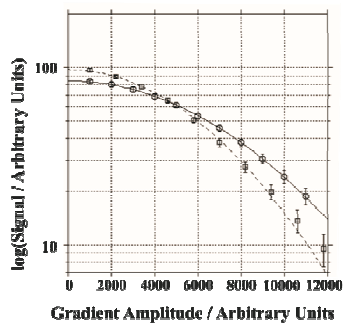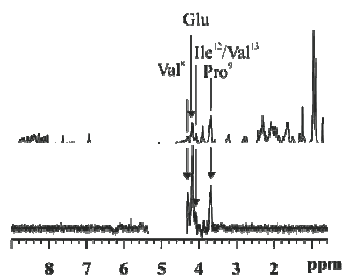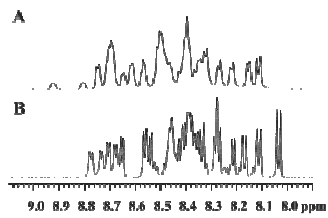51
52
53
54
55
56
57
58
59
60

FIGURE 2

FIGURE 3

1
2
3
4
5
6
7
8
9
10
11
12
13
14
15
16
17
18
19
20
21
22
23
24
25
26
27
28
29
30
31
32
33
34
35
36
37
38
39
40
41
42
43
44
45
46
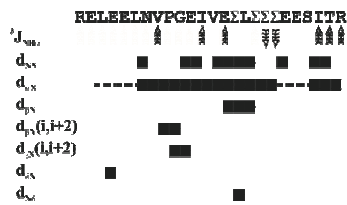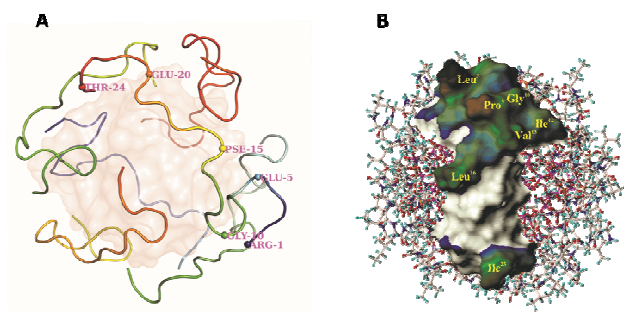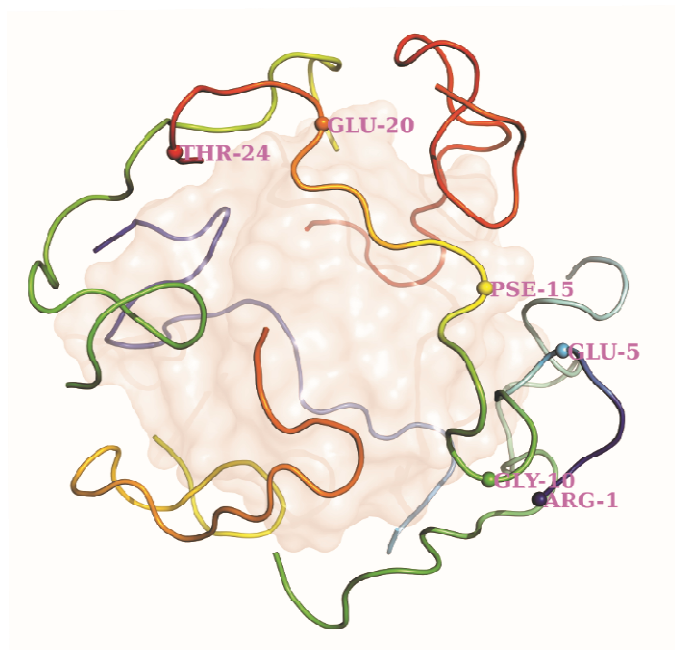47
48
49
50
51
52
53
54
55
56
57
58
59
60

FIGURE 4

A

B

FIGURE 5

1
2
3
4
5
6
7
8
9
10
11
12
13
14
15
16
17

FIGURE 6

18
19
20
21
22
23
24
25
26
27
28
29
30
31
32
33
34
35
36
37
38
39
40
41
42
43
44
45
46
47
48
49
50
51
52
53
54
55
56
57
58

43

59
60

FIGURE 7

FIGURE 8

TABLE OF CONTENTS GRAPHIC

Author/s:
Cross, KJ; Huq, NL; Reynolds, EC

Title:
Casein Phosphopeptide-Amorphous Calcium Phosphate Nanocomplexes: A Structural Model

Date:
2016-08-09

Persistent Link:
http://hdl.handle.net/11343/161187

File Description:
Accepted version